Electrical Engineering (2019) 101:921–933
https://doi.org/10.1007/s00202-019-00831-8

ORIGINAL PAPER

Temperature calculation of overhead power line conductors based on CIGRE Technical Brochure 601 in Slovakia

Martin Kanálik[1] · **Anastázia Margitová**[1] · **Ľubomír Beňa**[1]

Received: 25 July 2019 / Accepted: 3 September 2019 / Published online: 20 September 2019

Abstract
An overhead power line is a structure used in the electric power system to transmit electrical energy. The performance of overhead power lines depends on their parameters. An important parameter of the power line in the power system is its thermal limit. This article deals with the temperature calculation of overhead power line ACSR conductors according to the methodology stated in CIGRE Technical Brochure 601: Guide for thermal rating calculations of overhead lines. The calculated temperature is also compared with the measurement under laboratory conditions and also on a real power line in the Slovakia power system. At the end of the article, the dynamic thermal rating of ACSR conductors depending on climatic conditions is also calculated. Obtained results are compared with ampacity limits for summer and winter season used by Slovak transmission system operators. The article also compares the CIGRE Technical Brochure 601 with its older version CIGRE Technical Brochure 207: Thermal behavior of overhead conductors.

Keywords Overhead power line · ACSR conductor · CIGRE Technical Brochure 601 · CIGRE Technical Brochure 207 · Dynamic thermal rating · Ampacity

1 Introduction

Overhead power line conductors are an integral part of the transmission power system. They operate at high voltages, so their parameters must meet certain limits to ensure safe operation. One of the most important factors that affect line operation is the temperature of conductors [1]. If the heat generated by the current flowing exceeds the thermal limit, the conductor will be irreversibly damaged. To avoid thermal damage of the power line conductors, it is necessary to determine the maximum current that can flow through conductors [2]. Ampacity is the main parameter of the overhead power line design and operation; this value is the maximum amount of electrical current that can flow through the power line (or conductor) without disturbing its mechanical and electrical properties [3]. Ampacity is determined by mechanical and electrical properties of the conductor, the ability of heat generation within a conductor and ambient conditions [4]. The weather conditions and conductor parameters (temperature, sag, clearance, tension, vibration) monitoring is discussed by Fernandez and his team [5]. Teh and Cotton [6] described the identification of critical spans for the optimal placement of climatic conditions sensors and conductor parameters sensors. Musilek et al. [7] analyzed the conductor thermal aging. The improving of transmission capability and identification of maximum loadability limits of overhead power lines are discussed by Quaia [8]. Medveď and his team analyzed the measuring of the magnetic field around power lines [9].

In some transmission power systems, different fixed and weather independent ampacity limits are used for the summer and winter seasons. The set current limits for the summer and winter seasons represent much lower values than the current values that can be loaded to power lines under the actual weather conditions [4, 10, 11]. Dynamic thermal rating (DTR) of transmission lines provides the actual ampacity of overhead lines based on real-time operating (weather/atmospheric) conditions. The main aim of DTR is to increase the ampacity of existing transmission lines, mitigate transmission line congestion, facilitate wind energy integration, enable economic benefits and improve the reliability performance of

✉ Anastázia Margitová
anastazia.margitova@tuke.sk

[1] Department of Electric Power Engineering, Faculty of Electrical Engineering and Informatics, Technical University of Košice, Letná 9, 042 00 Kosice, Slovak Republic

power systems [12]. There are many articles [3, 13–17] dealing with DTR models of overhead transmission power lines. Kosec [18], Pytlak [19] and their colleagues dealt with the DTR modeling with consideration of precipitation. DTR can be determined for a steady state as well as the transient state.

Several industrial standards deal with the calculation of the temperature and ampacity of overhead power line conductors. The most commonly used methods are described in the IEEE Standard for calculating the current–temperature relationship of bare overhead conductors [20], CIGRE Technical Brochure 207 [21] (2002) and its extended version CIGRE Technical Brochure 601 [22] (2014). According to Schmidt [23], these methods provide similar results and they can be considered equivalent (the author compared the 1993 IEEE standard version with the 1992 CIGRE standard version). Many other studies [13, 15, 24, 25] deal with the comparison of IEEE and CIGRE standards for calculating the conductor ampacity. In this paper, we analyze the ampacity of overhead conductors using the CIGRE standards [21, 22].

2 Dynamic thermal rating calculation according to CIGRE Technical Brochure 601

The CIGRE (International Council on Large Electric Systems) Technical Brochure (TB) 601 is the updated and extended version of the CIGRE Technical Brochure 207 [21, 22]. The TB 207 deals with the thermal behavior of overhead power line conductors at low current densities (< 1.5 A/mm^2) and low temperatures (< 100 °C). The objective of the TB 601 is to calculate the thermal rating of overhead lines, including those lines operated at high current densities and temperatures. The TB 601 takes into account variations in weather conditions or current with time and also higher currents and higher temperatures of overhead power line conductors [22]. Therefore, in addition to steady state (weather conditions and conductor parameters are fairly constant over time), this standard also considers the transient state. According to CIGRE TB 601 [22], for a steady state (weather variables, conductor current and temperature remain constant), the thermal equilibrium of the conductor with consideration of actual weather conditions can be expressed by the power balance equation, where the left part of this equation is represented by the quantities/powers (W/m) causing the heating of the conductor (increasing the temperature of the conductor) and the right part of the equation is characterized by quantities/powers (W/m) causing the cooling of the conductor:

$$P_j + P_s = P_c + P_r, \tag{1}$$

where P_j is the heating of the conductor by the current flowing (Joule heating), P_s is the heating of the conductor by the sunlight (solar heating), P_c is the cooling of the conductor by the convection (convective cooling, natural and forced convection), P_r is the cooling of the conductor by the radiation (radiative cooling).

In the case of heavily loaded lines, Joule heating is a major factor in determining the conductor ampacity [12]. Joule heating represents the energy generated by the current flowing through the conductor. It takes into account the direct current resistance and the skin effect (in the case of alternating currents). The Joule heat gain [22] P_j (W/m) is calculated by:

$$P_j = I_{AC}^2 R_{AC\,20}\left[1 + \alpha\left(T_s - 20\right)\right], \tag{2}$$

where I_{AC} is the root-mean-square (RMS) value of the AC current flowing through the conductor (A), $R_{AC\,20}$ is the conductor AC (including skin effects) resistance at 20 °C (Ω/m), α is the temperature coefficient of resistance (K^{-1} or °C^{-1}), T_s is the conductor temperature (°C).

The effect of the solar heating on the ampacity of power line conductors is discussed by Liu and his team [26]. The solar heating [22] P_s (W/m) can be written as:

$$P_s = \alpha_s S D, \tag{3}$$

where α_s is the absorptivity coefficient of conductor surface (dimensionless), S is the intensity of solar radiation (W/m^2), D is the conductor outer diameter (m).

The value of the absorptivity coefficient of the conductor surface varies from 0.2 for a bright new conductor to 0.9 for a weathered conductor in an industrial environment. For a new conductor in the heavy industrial environment the absorptivity coefficient is around 0.5 after exposure for approximately one month, and around 0.9 after about one year [22]. For most purposes, a value of 0.5 may be used for this coefficient [21].

Convection is almost always the most important factor affecting the cooling of overhead conductors, even for still air conditions (zero wind speed). There is natural and forced convection. Natural convection occurs at zero wind speed or wind speeds below 0.5 m/s acting along the line. Forced convection occurs in the case of wind action and has a significantly greater cooling effect (compared to natural convection) [22]. The effect of wind speed and direction on the ampacity of power line conductors is studied by Ding and his colleagues [27]. In addition to some of the above-mentioned parameters, the following parameters [21, 22] are useful in calculating convective heat transfer:

(a) gravitational acceleration g (m/s^2), $g = 9.81$ m/s^2,
(b) height above sea level y (m),
(c) wind velocity V (m/s),
(d) angle of attack (angle between wind direction and the axis of the conductor) δ (°),

(e) outer layer wire diameter of the conductor (in the case of ACSR conductors it is an aluminum wire) d (m),
(f) specific heat capacity of air c_f (J/kg K), $c_f = 1005$ J/kg K,
(g) ambient temperature T_a (°C),
(h) film temperature (conductor surface layer temperature) T_f (°C),

$$T_f = 0.5\left(T_s + T_a\right), \tag{4}$$

(i) conductor surface roughness R_f (dimensionless),

$$R_f = d/\left[2(D-d)\right], \tag{5}$$

(j) dynamic viscosity of air μ_f (kg/m s),

$$\mu_f = \left(17.239 + 4.635\times10^{-2}T_f - 2.03\times10^{-5}T_f^2\right)\times10^{-6}, \tag{6}$$

(k) density of air γ_f (kg/m^3),

$$\gamma_f = \left(1.293 - 1.525\times10^{-4}y + 6.379\times10^{-9}y^2\right)\Big/\left(1 + 0.00367T_f\right), \tag{7}$$

(l) relative density of air γ_r (dimensionless),

$$\gamma_r = \exp\left(-1.16\times10^{-4}y\right), \tag{8}$$

(m) kinematic viscosity of air v_f (m^2/s),

$$v_f = 1.32\times10^{-5} + 9.5\times10^{-8}T_f \text{ [21]}, \tag{9}$$

$$v_f = \mu_f/\gamma_f \text{ [22]}, \tag{10}$$

(n) thermal conductivity of air λ_f (W/m K),

$$\lambda_f = 2.42\times10^{-2} + 7.2\times10^{-5}T_f \text{ [21]}, \tag{11}$$

$$\lambda_f = 2.368\times10^{-2} + 7.23\times10^{-5}T_f - 2.763\times10^{-8}T_f^2 \text{ [22]}, \tag{12}$$

(o) Prandtl number Pr (dimensionless),

$$Pr = 0.715 - 2.5\times10^{-4}T_f \text{ [21]}, \tag{13}$$

$$Pr = c_f\mu_f/\lambda_f \text{ [22]}, \tag{14}$$

(p) Reynolds number Re (dimensionless),

$$Re = \rho_r VD/v_f \text{ [21]}, \tag{15}$$

$$Re = VD/v_f \text{ [22]}, \tag{16}$$

(q) Grashof number Gr (dimensionless),

$$Gr = D^3\left(T_s - T_a\right)g/\left[\left(T_f + 273\right)v_f^2\right], \tag{17}$$

(r) Nusselt number for forced convection and 90° angle between wind direction and the conductor axis $Nu_{90°}$ (dimensionless),

$$Nu_{90°} = B_1(Re)^n, \tag{18}$$

(s) Nusselt number for forced convection and different angles between wind direction and the conductor axis Nu_δ (dimensionless),

$$Nu_\delta = Nu_{90°}\left[A_1 + B_2(\sin\delta)^{m_1}\right], \tag{19}$$

(t) Nusselt number for natural convection Nu_0 (dimensionless),

$$Nu_0 = A_2(Gr\times Pr)^{m_2}. \tag{20}$$

B_1 and n are constants depending on the Reynolds number and conductor surface roughness, found in Table 1. The values of the constants A_1, B_1, m_1 are given in Table 2. Constants A_2 and m_2 depend on the product of Grashof and

Table 2 Constants A_1, B_1 and m_1 for calculation of forced convective heat transfer

CIGRE Technical Brochure 601				
Smooth conductors	CIGRE Technical Brochure 207			
	Stranded conductors			
	Angle of attack	A_1	B_1	m_1
$Nu_\delta = Nu_{90°}\left[\left(\sin^2\delta + 0.0169\cos^2\delta\right)^{0.225}\right]$ (22)	$0° < \delta \le 24°$	0.42	0.68	1.08
	$24° < \delta \le 90°$	0.42	0.58	0.90

Table 1 Constants B_1 and n for calculation of forced convective heat transfer

CIGRE Technical Brochure 601								
Smooth conductors			CIGRE Technical Brochure 207					
			Stranded conductors $R_f \le 0.05$			Stranded conductors $R_f > 0.05$		
Re	B_1	n	Re	B_1	n	Re	B_1	n
$35–5\times10^3$	0.583	0.471	100–2650	0.641	0.471	100–2650	0.641	0.471
$5\times10^3–5\times10^4$	0.148	0.633	$2650–5\times10^4$	0.178	0.633	$2650–5\times10^4$	0.048	0.800
$5\times10^4–2\times10^5$	0.0208	0.814						

Prandtl numbers; they are given in Table 3 [22]. The convective heat loss [22] P_c (W/m) is given by:

$$P_c = \pi \lambda_f (T_s - T_a) Nu, \tag{21}$$

where the Nusselt number Nu can be found from Eq. (18), (19) or (22) for forced convection, or from Eq. (20) for natural convection, respectively.

The radiation loss P_r (W/m) is the total radiative energy transmitted from the conductor surface. It can be divided into two components: the heat radiated to the ground and surroundings, and the heat radiated directly to the sky. Applying the Stefan–Boltzmann law, the radiative cooling [22] can be expressed as:

$$P_r = \pi D \varepsilon_s \sigma_B \left[(T_s + 273)^4 - (T_a + 273)^4 \right], \tag{23}$$

where ε_s is the emissivity coefficient of conductor surface (dimensionless) and σ_B is the Stefan–Boltzmann constant (W/m^2 K^4), $\sigma_B = 5.6697 \cdot 10^{-8}$ W/m^2 K^4.

The value of the emissivity coefficient of the conductor surface varies from 0.2 to 0.3 for a new conductor to 0.8–0.9 for a weathered conductor in industrial or heavy agricultural environments [22]. For most purposes, a value of 0.5 may be used for this coefficient [21].

Based on the power balance Eq. (1) and Eq. (2), the value of the DTR [4] of the conductor the temperature of which does not exceed temperature T_s is determined by:

$$I_{max} = \sqrt{\frac{P_c + P_r - P_s}{R_{AC\,20}\left[1 + \alpha (T_s - 20)\right]}}. \tag{24}$$

On the other hand, Eqs. (1) to (24) can also be used to determine a steady-state conductor temperature T_s at a given (measured) current flowing I_{meas} through the conductor. In this case, it is necessary to apply an iteration procedure. We can calculate the current values I_{max} by increasing or decreasing the initial conductor temperature value T_s. The iteration process can be stopped when the calculated current value I_{max} is equal with sufficient accuracy to the actual (measured) current value I_{meas}. The calculated temperature value T_s then represents the steady-state conductor temperature at given climatic conditions and measured current I_{meas}. The flowchart illustrating the algorithm of the conductor temperature calculation at a known current flowing through the conductor is shown in Fig. 1, where ΔI is the required deviation of the calculated current I_{max} from the measured current I_{meas} (in our case we considered $\Delta I = 1$ A), ΔT_+ is the temperature change if an increase in conductor temperature T_s is needed (in our case we considered $\Delta T_+ = 0.01$ °C), ΔT_- is the temperature change if a decrease in conductor temperature T_s is needed (in our case we considered $\Delta T_- = 0.003$ °C).

Table 3 Constants A_2 and m_2 for calculation of natural convective heat transfer

	$Gr \times Pr$		A_2	m_2
	from	to		
CIGRE 601	10^{-1}	10^{2}	1.02	0.148
CIGRE 207	10^{2}	10^{4}	0.850	0.188
	10^{4}	10^{7}	0.480	0.250
	10^{7}	10^{12}	0.125	0.333

3 Comparison of the temperature calculated by CIGRE Technical Brochure 601 with real temperature measurement on ACSR conductors under laboratory conditions

There are similar studies [14–16] comparing the measured temperature of overhead conductors in laboratory conditions with the temperature calculated by the CIGRE (or IEEE) standard. For comparison of the temperature calculated by CIGRE TB 601 (or CIGRE TB 207) described in the previous section with real measurement, several temperature measurements were performed for two ACSR conductors (350 AlFe 6 and 450 AlFe 8). The technical parameters of these ACSR conductors are shown in Table 4. Temperature measurements were carried out in a laboratory using simulation without and with the presence of wind (speed 2 m/s at a 90° angle of attack). Ambient temperature was recorded at these measurements, assuming height above sea level of 208 m and intensity of solar radiation of 0 W/m^2 (without the influence of solar heating).

Measurements were carried out from the ambient conductor temperature to the steady-state conductor temperature at different steady-state RMS values of the current flowing through the conductor. Two of these current and temperature measurements of the conductor 350 AlFe 6 for a current of 600 A and the conductor 450 AlFe 8 for a current of 800 A are shown in Figs. 2 and 3. In the first step, the conductor temperature was determined without considering the influence of wind. In the second step, the presence of wind was simulated for the same conductor and approximately the same current value.

Table 5 shows the comparison of measured and calculated (according to the TB 601 and TB 207) temperatures of two analyzed ACSR conductors. The higher the current flowing through the conductor, the higher the conductor temperature. It is also evident from Table 5 that with a wind speed 2 m/s, the conductors (350 AlFe 6 and 450 AlFe 8) can be loaded with a higher current than in the

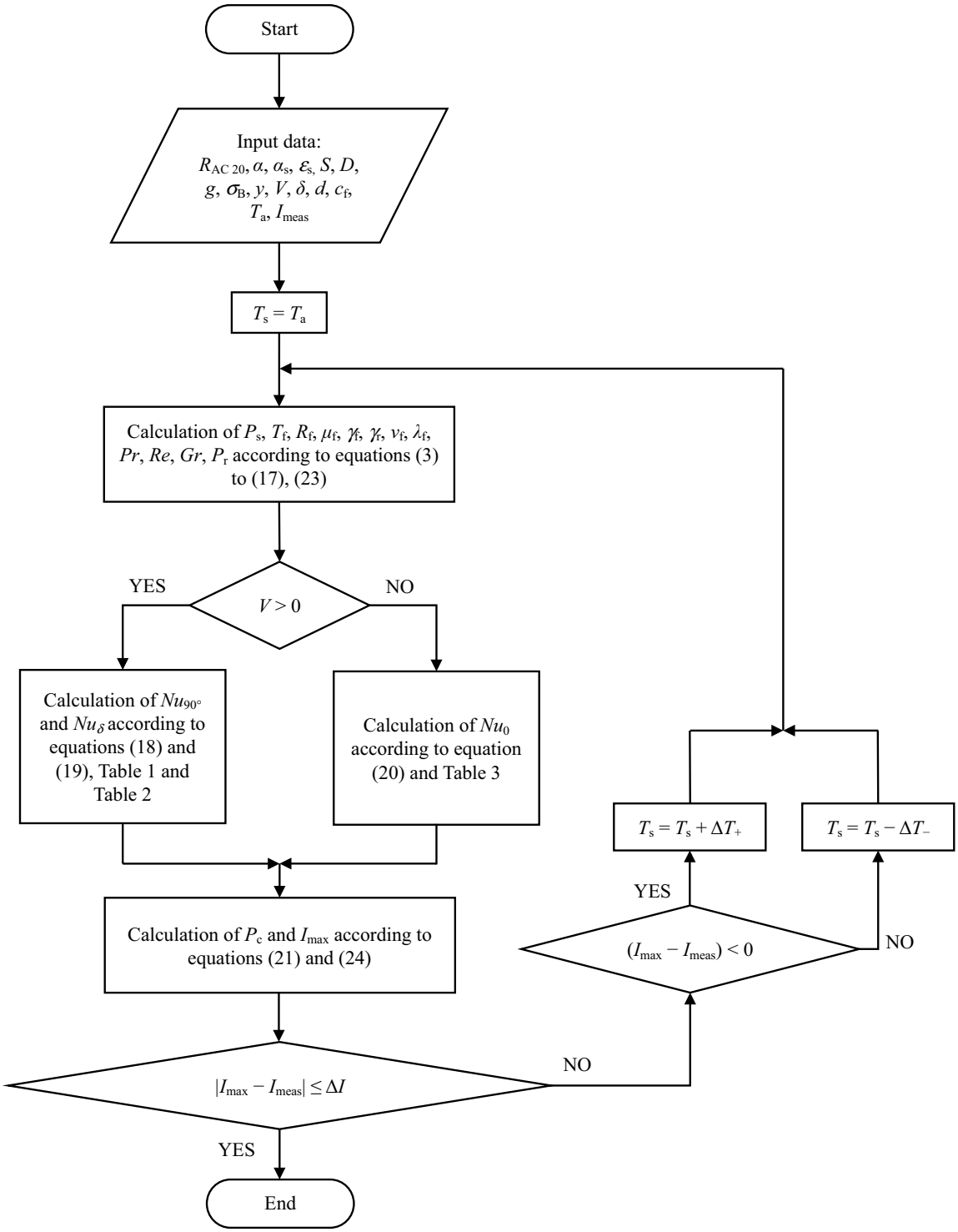

Fig. 1 Flowchart illustrating the algorithm of the conductor temperature calculation according to the CIGRE Technical Brochure 601 used in this paper

case of no wind. For example, in the case of the conductor 450 AlFe 8, a current of 800 A was flowing through it and its temperature without considering the wind influence was 77.2 °C, while in the case of wind influence with speed 2 m/s the temperature was only 39.6 °C.

For the 350 AlFe 6 conductor, the highest difference between the measured and calculated temperature was 1.47 °C (according to TB 207) and 1.33 °C (according to TB 601) at a current of 505 A with considering the wind speed 2 m/s. Temperature differences for other current values were

Table 4 Technical specification of analyzed ACSR conductors

Type of ACSR conductor	350 AlFe 6	450 AlFe 8
Conductor outer diameter (mm)	26.5	28.7
Outer layer wire diameter (mm)	4.0	3.75
AC resistance at 20 °C (Ω/km)	0.0816	0.0674
Temperature coefficient of resistance (K^{-1})	4.03×10^{-3}	
Absorptivity and emissivity coefficient (−)	0.35	

less than 1 °C (for 350 AlFe 6). In the case of the 450 AlFe 8 conductor, the highest temperature differences were 2.44 °C (according to TB 207, wind presence, current 805 A) and 2.9 °C (according to TB 601, without wind influence, current 1006 A). When comparing the two analyzed conductors (350 AlFe 6 and 450 AlFe 8), lower temperature differences were achieved for the conductor 350 AlFe 6.

Figures 4, 5, 6 and 7 show temperature dependencies on the RMS current flowing through the two analyzed conductors at wind speed 0 m/s and 2 m/s (90° angle of attack) and intensity of solar radiation 0 W/m^2 (calculated according to the TB 601 and TB 207). Figures 4, 5, 6 and 7 also show the actual measured current and temperature values of the analyzed conductors (also shown in Table 5). In the case of calculation of temperature–current dependencies, differences between measured and calculated temperature values were also caused by considering only one (average) temperature value (23 °C for no-wind simulation, 24 °C for 350 AlFe 6 and considering wind influence, 25 °C for 450 AlFe 8 and considering wind influence). Temperature calculation according to the TB 207 and TB 601 does not differ too much. The basic equations in these standards (TB) are the same, but the TB 601 considers more precise equations for some of the variables needed to calculate the conductor temperature (listed in the previous section).

4 Comparison of the temperature calculated by CIGRE Technical Brochure 601 with real temperature measurement on ACSR conductors of the real overhead power line

This section presents the calculation of temperature time variations of the real power line conductor based on ambient conditions and measured RMS current according to the CIGRE Technical Brochure 601. Similar research is described by several other authors [3, 13, 15–18]. Analyzed power line (voltage level 400 kV, length 90 km) was located between two electric power stations in the Slovak Republic (height above sea level of 113 m and 216 m). ACSR conductor (350 AlFe 6, Table 4) in triple bond configuration was used in the one section of the analyzed power line. Temperature calculations were realized in

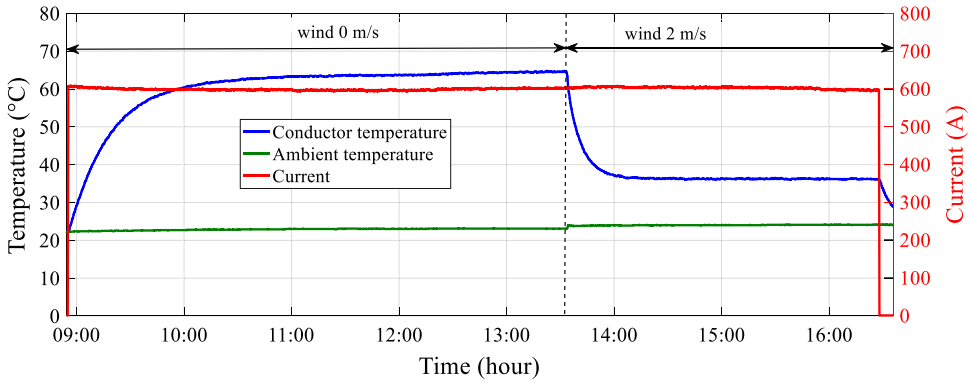

Fig. 2 Current and temperature time variations during real measurement with the conductor 350 AlFe 6

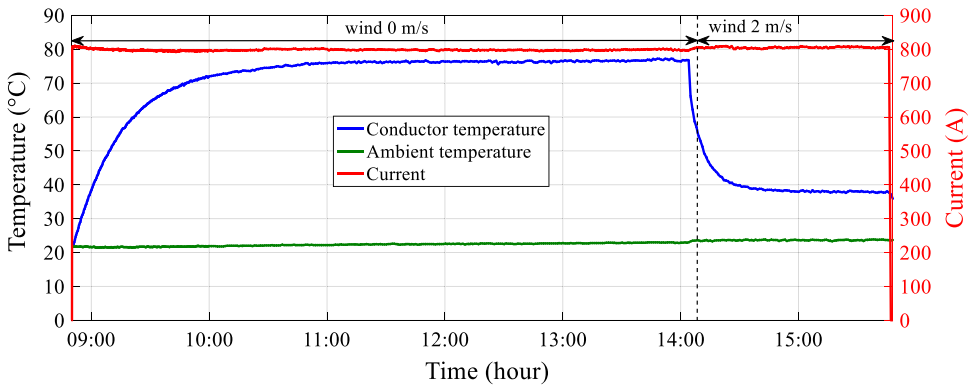

Fig. 3 Current and temperature time variations during real measurement with the conductor 450 AlFe 8

Table 5 Measured and calculated temperature of two analyzed ACSR conductors

Type of ACSR conductor	Wind speed (m/s)	Ambient temperature (°C)	Measured current (A)	Measured temperature (°C)	Calculated temperature TB 207 (°C)	Calculated temperature TB 601 (°C)
350 AlFe 6	0	21.9	301	33.6	33.86	34.05
		22.3	500	52.4	51.68	52.16
		23.1	500	52.8	52.52	53.00
		23.1	600	64.4	64.14	64.83
		23.1	600	64.8	64.14	64.83
		23	701	78	77.89	78.84
	2	23	505	32.4	30.93	31.07
		24	508	32.4	32.07	32.21
		24.2	597	36.1	35.51	35.71
		24.1	600	36.1	35.53	35.73
		23.5	701	40.2	39.36	39.63
		24.4	1006	60.1	59.96	60.59
450 AlFe 8	0	24.3	600	57.2	56.83	57.36
		24.3	610	58.2	57.82	58.37
		22.9	800	77.2	78.21	79.17
		24	810	80	80.72	81.71
		23.6	981	108	105.66	107.21
		23.7	1006	108.7	109.94	111.60
	2	25.6	604	34.1	34.53	34.69
		25.5	605	33.9	34.46	34.61
		24.9	800	39.6	41.01	41.29
		23.8	805	37.6	40.04	40.32
		24.3	1015	49.5	51.37	51.84
		24.5	1020	53.2	51.90	52.38

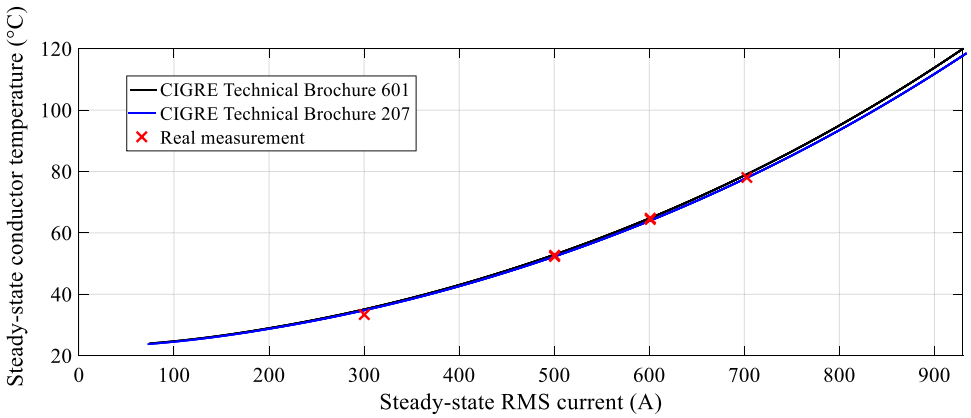

Fig. 4 Steady-state temperature dependence on the RMS current flowing through the conductor 350 AlFe 6 at a wind speed 0 m/s, intensity of solar radiation 0 W/m^2 and ambient temperature 23 °C

2018 for three days (Day 1, Day 2 and Day 3) with different climatic conditions. Two different measuring devices were installed in one of the electric stations (216 m a.s.l.) and recorded the ambient temperature, intensity of the solar radiation, RMS current flowing through the analyzed power line (conductor 350 AlFe 6), temperature of the conductor 350 AlFe 6 and wind speed. Measured data were obtained with a recording interval of 15 min.

Time variations of measured RMS currents flowing through the analyzed power line (through the conductor 350 AlFe 6), for each analyzed day, are shown in Fig. 8. Figures 9, 10 and 11 show the measured intensity of solar radiation, wind speed and ambient temperature for three analyzed days necessary for the calculation of the actual temperature of the conductor 350 AlFe 6.

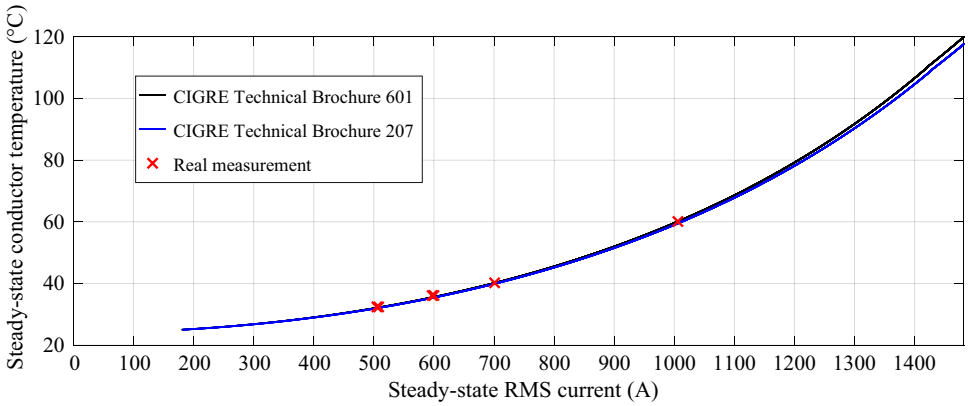

Fig. 5 Steady-state temperature dependence on the RMS current flowing through the conductor 350 AlFe 6 at a wind speed 2 m/s (90° angle of attack), intensity of solar radiation 0 W/m^2 and ambient temperature 24 °C

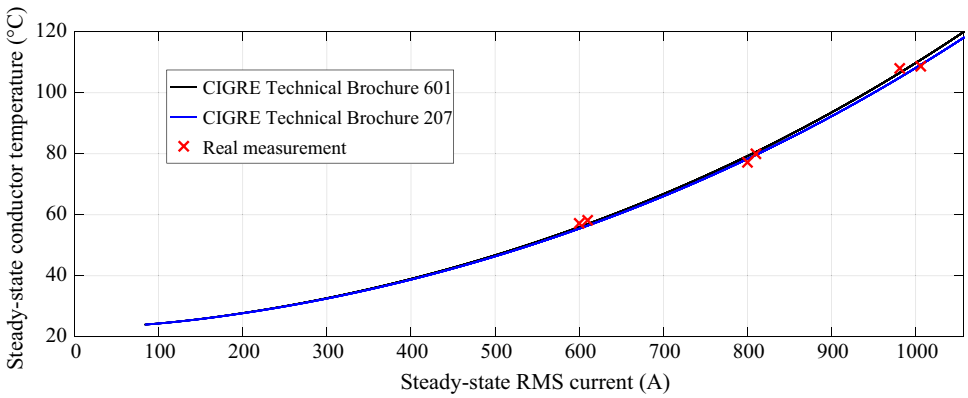

Fig. 6 Steady-state temperature dependence on the RMS current flowing through the conductor 450 AlFe 8 at a wind speed 0 m/s, intensity of solar radiation 0 W/m^2 and ambient temperature 23 °C

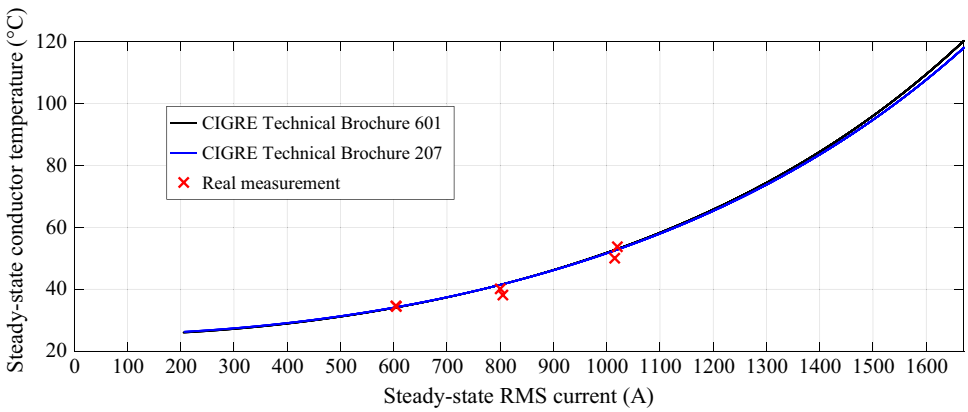

Fig. 7 Steady-state temperature dependence on the RMS current flowing through the conductor 450 AlFe 8 at a wind speed 2 m/s (90° angle of attack), intensity of solar radiation 0 W/m^2 and ambient temperature 25 °C

Figures 12, 13 and 14 show the comparison of the measured and calculated temperature of the conductor 350 AlFe 6 for Day 1, Day 2 and Day 3. Since the wind angle was not available for the data provided, conductor temperature calculations were realized particularly for a 0°, 45° and 90° angle of attack. The best correlation with the measured data was achieved when considering a wind angle of 45°. The deviation of the calculated temperature of the conductor 350 AlFe 6 from the measured values was ranged:

- from −2.5 to 2.9 °C for Day 1 (Fig. 12), the mean deviation of 0.2 °C,
- from −0.9 to 3.4 °C for Day 2 (Fig. 13), the mean deviation of 1 °C,
- from −1.7 to 5.7 °C for Day 3 (Fig. 14), the mean deviation of 3.4 °C.

Figures 12, 13 and 14 show that the wind direction has no significant effect on differences between the measured and calculated temperature. In the paper, we calculated the

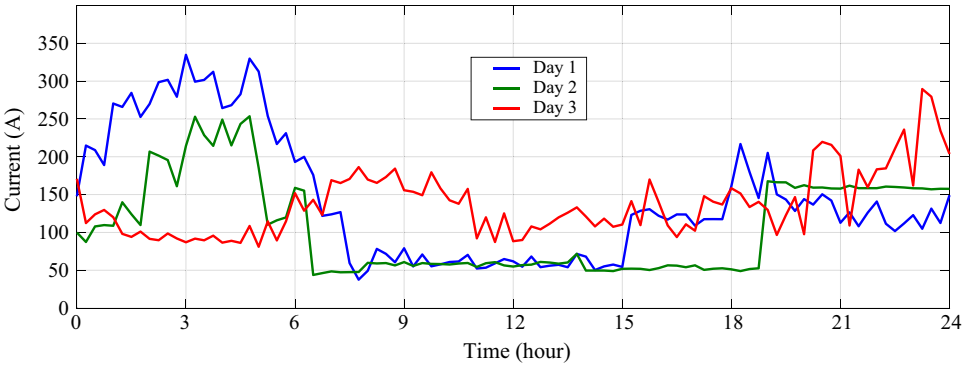

Fig. 8 Time variation of the measured RMS current flowing through the analyzed power line during Day 1, Day 2 and Day 3

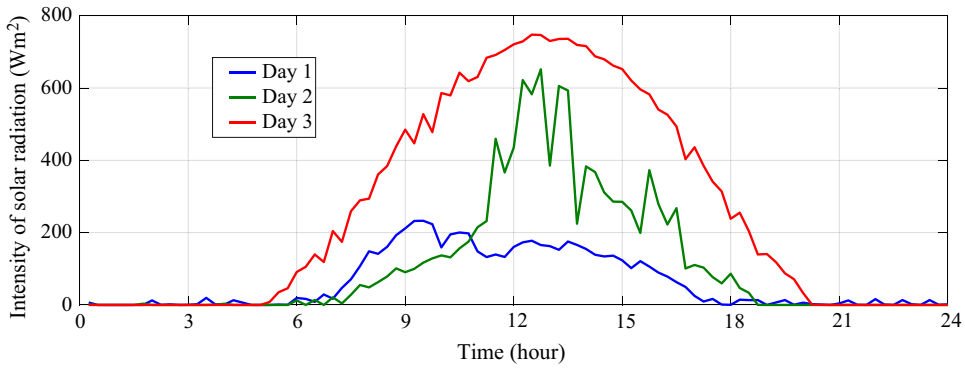

Fig. 9 Time variation of the measured intensity of solar radiation during Day 1, Day 2 and Day 3

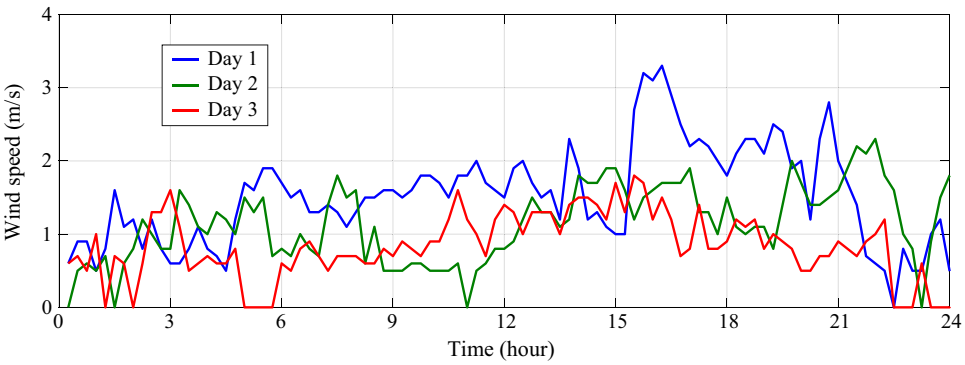

Fig. 10 Time variation of the measured wind speed during Day 1, Day 2 and Day 3

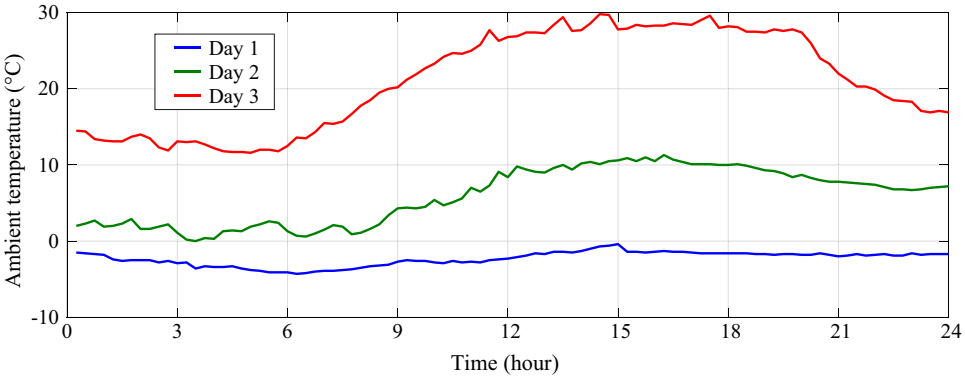

Fig. 11 Time variation of the measured ambient temperature during Day 1, Day 2 and Day 3

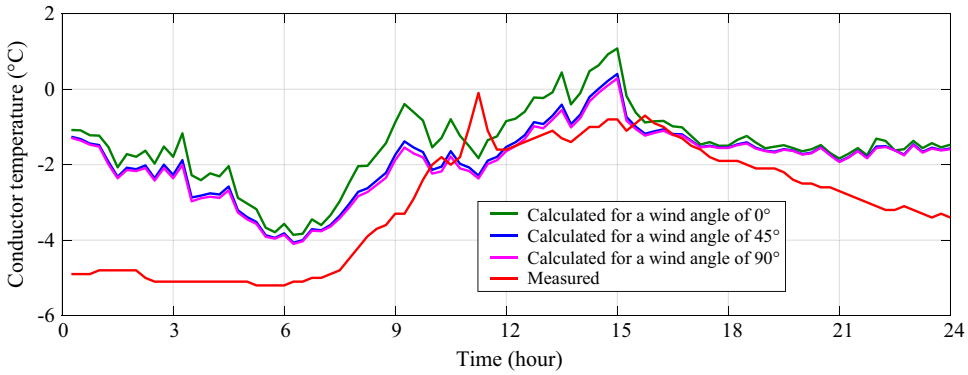

Fig. 12 Comparison between measured and calculated temperature of the conductor 350 AlFe 6 for Day 1

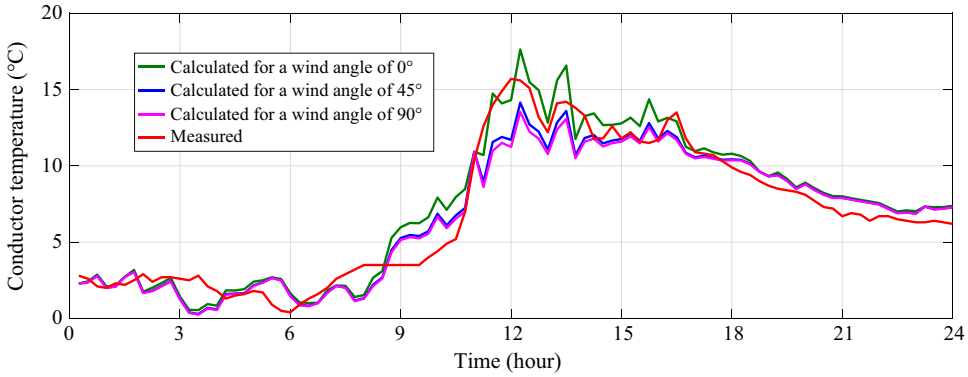

Fig. 13 Comparison between measured and calculated temperature of the conductor 350 AlFe 6 for Day 2

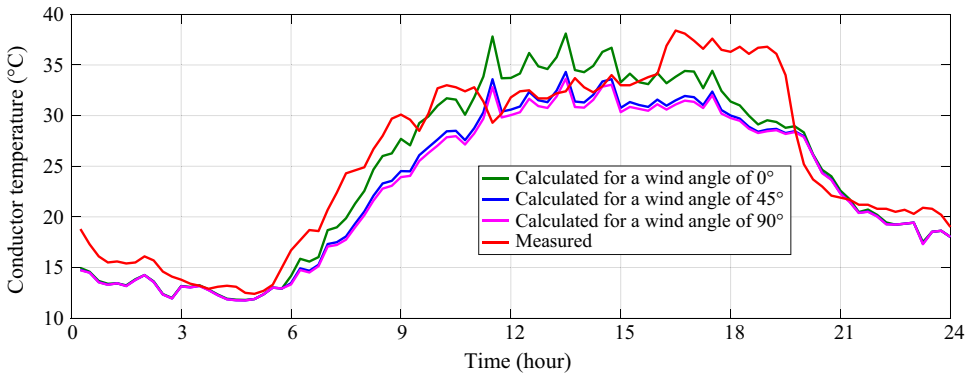

Fig. 14 Comparison between measured and calculated temperature of the conductor 350 AlFe 6 for Day 3

steady-state temperature for every 15 min and we considered constant conditions for the given 15-min interval. If the RMS current or ambient conditions change, the conductor temperature gradually increases/decreases. Temperature stabilization under the new constant conditions can occur after more than 15 min, for example after 30 or 45 min (see Figs. 2 and 3 from real measurement in laboratory conditions, where temperature stabilization occurred after about two hours). This fact also caused a difference between the measured and calculated temperature values.

5 Dynamic thermal rating calculation of real overhead power line conductors

In this section, we carried out calculations of DTR using a steady-state thermal model for each 15 min of Day 3, realized for the analyzed power line (conductor 350 AlFe 6). These calculations were provided to achieve the maximum conductor operating temperature of 80 °C based on the TB 601.

Figures 15 and 16 show the time variation of the calculated DTR of the conductor 350 AlFe 6 with and without consideration of the wind influence. Limits marked with the red and magenta lines are used by Slovak transmission

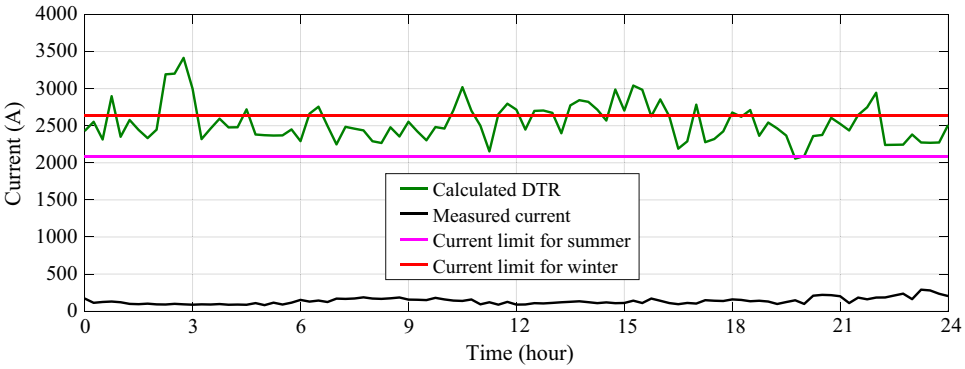

Fig. 15 Time variation of the calculated DTR of the conductor 350 AlFe 6 with wind influence consideration for Day 3

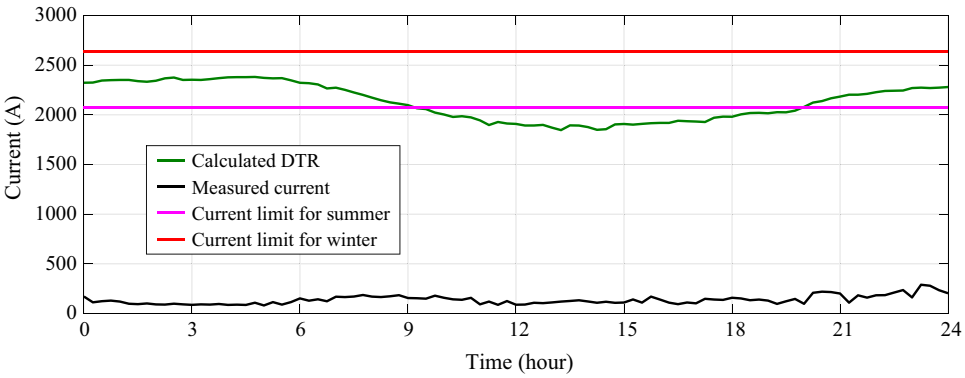

Fig. 16 Time variation of the calculated DTR of the conductor 350 AlFe 6 without wind influence consideration for Day 3

system operators in the present as summer and winter season current limits. In the case of the wind influence consideration (Fig. 15), it is possible to observe that the calculated current was above the current limit stated by transmission system operators for most of the day during the summer season. In the case of 350 AlFe 6 conductor, without consideration of the wind influence (Fig. 16), it is possible to observe that the calculated current was below current limit stated by transmission system operators for the winter season.

Figures 15 and 16 show that the current flowing through the analyzed power line was low compared with limits used by Slovak transmission system operators. Thus, the effect of the current flowing through the analyzed power line on the conductor temperature was low. On the other hand, the influence of ambient conditions on the conductor temperature was more pronounced.

6 Conclusion

With an increasing demand for electric power, it is necessary to transfer that produced electricity to the end consumers. When transmitting electrical energy, climatic conditions (solar radiation, ambient temperature, wind, etc.) act on the power line conductors. Important parameters of the power line conductors are their temperature as well as the ampacity and these two parameters are interconnected. The mathematical description of climatic conditions influence on power line conductors is stated in CIGRE TB 601. The main objective of this article was to analyze this standard (TB) to determine the conductor DTR, taking into account actual climatic conditions.

The most widely used conductors of transmission power lines are ACSR (or AlFe) conductors, the conductive part of which is aluminum. Manufacturers specify the maximum operating temperature of ACSR conductors in the range of 90–110 °C. Part 1 of the standard STN EN 50341-1: Overhead electrical lines exceeding AC 45 kV [28] determines the maximum temperature of the conductor, where it is recommended to choose no less than 70 °C. This standard states the maximum current flowing for the specified maximum temperature for conservative climatic conditions: high ambient temperature (35 °C), high intensity of solar radiation (1000 W/m^2), low wind speed (0.5 m/s, 45° angle of attack) and absorption and emissivity coefficient 0.5. Based on long-term measurements of climatic conditions (temperature, wind) around power lines, it can be stated that for most of the year, these weather conditions do not reach the limit values as defined by the standard STN EN 50341-1.

In the first step, the measurements of the two ACSR conductor temperatures were made depending on the current flowing through these conductors (350 AlFe 6 and 450 AlFe 8) and comparing it with the temperatures

calculated according to CIGRE TB 601. In the case of the analyzed ACSR conductors, these were not new conductors, but rather conductors with moderate soiling. The emissivity and absorptivity coefficients for these conductors were set to 0.35. At this value of the absorptivity and emissivity coefficient, we achieved the best correlation of the measured data as compared with the calculated values. This corresponds approximately to the theoretical assumptions given in TB 601 where the values of these coefficients range from 0.2 for new conductors to 0.9 for weathered conductors in industrial environments.

In the second part of this article, the calculated and measured values of the conductor temperatures were compared to a real power line for three specific days. Data of climatic conditions, actual conductor temperature and the current flowing through the conductor (recorded every 15 min) were known. Based on the obtained results, it can be said that the CIGRE TB 601 is applicable for approximate calculation of the DTR for the 15-min interval.

As has been shown during temperature measurement in laboratory conditions with a significant change in either climatic conditions or RMS current value, the conductor temperature can be stabilized within a time range of one to two hours. Since there are no dramatic changes in climatic and RMS current conditions over 15 min in real conditions in general, this methodology is applicable for a 15-min evaluation. Based on the above, the time variations of the DTR for one particular day were shown at the end of the article.

Acknowledgements This work was supported by the Scientific Grant Agency of the Ministry of Education of Slovak Republic and the Slovak Academy of Sciences under the contract VEGA No. 1/0372/18.

Compliance with ethical standards

Conflicts of interest The authors declare that they have no conflict of interest.

References

1. Beryozkina S, Sauhats A, Vanzovichs E (2011) Climate conditions impact on the permissible load current of the transmission line. In: Proceedings of the IEEE Trondheim PowerTech, pp 1–6
2. Yan Z, Wang Y, Liang L (2017) Analysis on ampacity of overhead transmission lines being operated. J Inf Process Syst 13:1358–1371
3. Šnajdr J, Sedláček J, Vostracký Z (2014) Application of a line ampacity model and its use in transmission lines operations. J Electr Eng 65:221–227
4. Kanálik M, Margitová A, Urbanský J, Beňa Ľ (2019) Temperature calculation of overhead power line conductors according to the CIGRE Technical Brochure 207. In: Proceedings of the 20th international scientific conference on electric power engineering (EPE), pp 24–28
5. Fernandez E, Albizu I, Bedialauneta M, Mazon A, Leite P (2016) Review of dynamic line rating systems for wind power integration. Renew Sustain Energy Rev 53:80–92
6. Teh J, Cotton I (2015) Critical span identification model for dynamic thermal rating system placement. IET Gener Transm Distrib 9(16):2644–2652
7. Musilek P, Heckenbergerova J, Bhuiyan M (2012) Spatial analysis of thermal aging of overhead transmission conductors. IEEE Trans Power Deliv 27(3):1196–1204
8. Quaia S (2018) Critical analysis of line loadability constraints. Int Trans Electr Energ Syst 24:1–11
9. Medveď D, Mišenčík L, Kolcun M, Zbojovský J, Pavlík M (2015) Measuring of magnetic field around power lines. In: Proceedings of the 8th international scientific symposium Elektroenergetika, pp 148–51
10. Heckenbergerova J, Musilek P, Filimonenkov K (2013) Quantification of gains and risks of static thermal rating based on typical meteorological year. Int J Electr Power Energy Syst 44(1):227–235
11. Heckenbergerova J, Musilek P, Filimonenkov K (2011) Assessment of seasonal static thermal ratings of overhead transmission conductors. In: Proceedings of the IEEE power and energy society general meeting, pp 1–8
12. Karimi S, Musilek P, Knight AM (2018) Dynamic thermal rating of transmission lines: a review. Renew Sustain Energy Rev 91:600–612
13. Arroyo A, Castro P, Martinez R et al (2015) Comparison between IEEE and CIGRE thermal behaviour standards and measured temperature on a 132-kV overhead power line. Energies 8(12):13660–13671
14. Fu J, Abbott S, Fox B, Morrow DJ, Abdelkader S (2010) Wind cooling effect on dynamic overhead line ratings. In: Proceedings of the 45th International Universities Power Engineering Conference (UPEC), pp 1–6
15. Abbott S, Abdelkader S, Bryans L, Flynn D (2010) Experimental validation and comparison of IEEE and CIGRE dynamic line models. In: Proceedings of the 45th International Universities Power Engineering Conference (UPEC), pp 1–5
16. Fu J, Morrow DJ, Abdelkader SM (2012) Integration of wind power into existing transmission network by dynamic overhead line rating. In: Proceedings of the 11th international workshop on large-scale integration of wind power into power systems, pp 1–5
17. Musavi M, Chamberlain D, Li Q (2011) Overhead conductor dynamic thermal rating measurement and prediction. In: Proceedings of the IEEE international conference on smart measurements of future grids (SMFG), pp 135–138
18. Kosec G, Maksić M, Djurica V (2017) Dynamic thermal rating of power lines—model and measurements in rainy conditions. Int J Electr Power Energy Syst 91:222–229
19. Pytlak P, Musilek P, Lozowski E, Toth J (2011) Modelling precipitation cooling of overhead conductors. Electric Power Syst Res 81:2147–2154
20. IEEE (2012) Standard for calculating the current-temperature relationship of bare overhead conductors. Std 738
21. CIGRE, Working Group 22.12 (2002) Thermal behaviour of overhead conductors, Technical Brochure 207
22. CIGRE, Working Group B2.43 (2014) Guide for thermal rating calculation of overhead lines, Technical Brochure 601
23. Schmidt N (1999) Comparison between IEEE and CIGRE ampacity standards. IEEE Trans Power Deliv 14:1555–1559
24. Michiorri A et al (2015) Forecasting for dynamic line rating. Renew Sustain Energy Rev 52:1713–1730
25. Simms M, Meegahapola L (2013) Comparative analysis of dynamic line rating models and feasibility to minimise energy losses in wind rich power networks. Energy Convers Manage 75:11–20
26. Liu G, Li Y, Liu S, Dong X, Qu F, Li Y (2016) Real-time solar radiation intensity modeling for dynamic rating of overhead transmission lines. In: Proceedings of the Australasian Universities Power Engineering Conference (AUPEC), pp 1–6

27. Ding Y, Gao M, Li Y et al (2016) The effect of calculated wind speed on the capacity of dynamic line rating. In: Proceedings of the IEEE international conference on high voltage engineering and application (ICHVE), pp 1–5
28. STN EN 50341-1: Overhead Electrical Lines Exceeding AC 45 kV. Part 1: General Requirements. Common Specifications (2013)